*Inorg. Chem.* **2007**, *46*, 3934–3945


# Mn(II) and Cu(II) Complexes of a Dithiadiazolyl Radical Ligand: Monomer/Dimer Equilibria in Solution

**James Britten,[†] Nigel G. R. Hearns,[‡] Kathryn E. Preuss,*[,‡] John F. Richardson,[§] and Sofi Bin-Salamon[||]**

*Department of Chemistry, McMaster University, 1280 Main Street West, Hamilton, Ontario L8S 4M1, Canada, Department of Chemistry, University of Guelph, 50 Stone Road East, Guelph, Ontario N1G 2W1, Canada, Department of Chemistry, University of Louisville, 2320 South Brook Street, Louisville, Kentucky 40292, and Department of Chemistry, North Carolina State University, Raleigh, North Carolina 27695*

Received October 11, 2006

Complexes of the 4-(2′-pyridyl)-1,2,3,5-dithiadiazolyl radical bidentate ligand with bis(hexafluoroacetylacetonato)-manganese(II) and with bis(hexafluoroacetylacetonato)copper(II) have been prepared. Unlike the previously reported cobalt(II) complex, these complexes form dimers via intermolecular S···S contacts in the solid state. The spectroscopic and magnetic properties of these species in the solid state and in solution are reported and compared to the previously reported Co(II) complex, with emphasis on the elucidation of the a monomer/dimer equilibrium in the solution. The electrochemical properties of these species in solution are also presented and discussed.

## Introduction

The development of molecule-based materials with interesting and potentially useful magnetic properties is one of the major goals in current synthetic research.[1] Many of the emerging molecule-based magnet designs use properties of paramagnetic transition metal ions mediated by specially designed organic ligands, including ligands that are themselves paramagnetic. Exchange interaction between unpaired electrons on a metal center and unpaired electrons on a spin-bearing ligand has been shown to effectively mediate longer range magnetic interactions between two coordinated metal centers. There are, however, relatively few spin-bearing ligands available. Currently, the majority of such ligands are varieties of semiquinone and its derivatives[2] or nitroxide,[3] including nitronyl nitroxides.[4] There has also been a notable contribution in the development of various verdazyl-based spin-bearing ligands,[5] 1,3,2-dithiazolyl ligands,[6] and the synthesis of an azaphenylenyl-based ligand.[7]

Recently, we demonstrated that the well-known 1,2,3,5-dithiadiazolyl (DTDA) radical[8] can be used as building blocks in the rational design of chelating spin-bearing ligands.[9,10] Herein, we begin to explore a property unique to

* To whom correspondence should be addressed. E-mail: kpreuss@uoguelph.ca.
[†] McMaster University.
[‡] University of Guelph.
[§] University of Louisville.
[||] North Carolina State University.

(1) (a) Gatteschi, D.; Sessoli, R.; Cornia, A. *Chem. Commun.* **2000**, 725. (b) Day, P. *J. Chem. Soc. Dalton Trans.* **2000**, 3483. (c) Blundell, S. J.; Pratt, F. L. *J. Phys.: Condens. Matter* **2004**, *16*, R771. (d) Mroziński, J. *Coord. Chem. Rev.* **2005**, *249*, 2534. (d) Miyasaka, H.; Nakata, K.; Lecren, L.; Coulon, C.; Nakazawa, Y.; Fujisaki, T.; Sugiura, K.; Yamashita, M.; Clérac, R. *J. Am. Chem. Soc.* **2006**, *128*, 3770.

(2) (a) Buchanan, R. M.; Pierpont, C. G. *J. Am. Chem. Soc.* **1980**, *102*, 4951. (b) Ray, K.; Weyhermüller, T.; Neese, F.; Wieghardt, K. *Inorg. Chem.* **2005**, *44*, 5345. (c) Bin-Salamon, S.; Brewer, S.; Depperman, E. C.; Franzen, S.; Kampf, J. W.; Kirk, M. L.; Kumar, R. K.; Lappi, S.; Peariso, K.; Preuss, K. E.; Shultz, D. A. *Inorg. Chem.* **2006**, *45*, 4461. (d) Hearns, N. G. R.; Korčok, J. L.; Paquette, M. M.; Preuss, K. E. *Inorg. Chem.* **2006**, *45*, 8817.

(3) (a) Caneschi, A.; Gatteschi, D.; Sessoli, R. *Acc. Chem. Res.* **1989**, *22*, 392. (b) Chiarelli, R.; Novak, M. A.; Rassat, A.; Tholence, J. L. *Nature* **1993**, *363*, 147. (c) Inoue, K.; Hayamizu, T.; Iwamura, H.; Hashizume, D.; Ohashi, Y. *J. Am. Chem. Soc.* **1996**, *118*, 1803.

(4) (a) Richardson, P. F.; Kreilick, R. W. *J. Am. Chem. Soc.* **1977**, *99*, 8183. (b) Lescop, C.; Belorizky, E.; Luneau, D.; Rey, P. *Inorg. Chem.* **2002**, *41*, 3375. (c) Caneschi, A.; Gatteschi, D.; Lalioti, N.; Sessoli, R.; Sorace, L.; Tangoulis, V.; Vindigni, A. *Chem. Eur. J.* **2002**, *8*, 286. (d) Yamada, S.; Yasui, M.; Nogami, T.; Ishida, T. *Dalton Trans.* **2006**, 1622.

(5) (a) Brook, D. J. R.; Lynch, V.; Conklin, B.; Fox, M. A. *J. Am. Chem. Soc.* **1997**, *119*, 5155. (b) Hicks, R. G.; Lemaire, M. T.; Thompson, L. K.; Barclay, T. M. *J. Am. Chem. Soc.* **2000,** *122*, 8077. (c) Barclay, T. M.; Hicks, R. G.; Lemaire, M. T.; Thompson, L. K. *Inorg. Chem.* **2001**, *40*, 5581. (d) Barclay, T. M.; Hicks, R. G.; Lemaire, M. T.; Thompson, L. K. *Inorg. Chem.* **2003**, *42*, 2261. (e) Koivisto, B. D.; Hicks, R. G. *Coord. Chem. Rev.* **2005**, *249*, 2612.

(6) (a) Fujita, W.; Awaga, K. *J. Am. Chem. Soc.* **2001**, *123*, 3601. (b) Fujita, W.; Awaga, K.; Kondo, R.; Kagoshima, S. *J. Am. Chem. Soc.* **2006**, *128*, 6016.

(7) Morita, Y.; Suzuki, S.; Fukui, K.; Nakazawa, S.; Sato, K.; Shiomi, D.; Takui, T.; Nakasuji, K. *Polyhedron* **2003**, *22*, 2215.



10.1021/ic0619456 CCC: $37.00 
Published on Web 04/19/2007

the DTDA-based ligand−metal coordination complexes, namely, the capacity for intermolecular interaction of the complexes via the sulfur atoms of the DTDA rings. We present the synthesis and characterization of the coordination complexes of bis(hexafluoroacetylacetonato)manganese (Mn(hfac)$_2$) and bis(hexafluoroacetylacetonato)copper (Cu(hfac)$_2$) with the spin-bearing 4-(2′-pyridyl)-1,2,3,5-dithiadiazolyl ligand **1**; complexes **2** and **3**, respectively. We compare the magnetic properties of the Mn and Cu complexes, in solution and in the solid state, to the magnetic properties of the previously reported Co complex **4**.

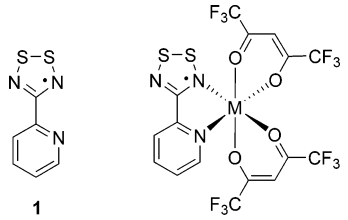


## Experimental Section

**General Considerations.** All preparations and manipulations were performed under an argon atmosphere using standard Schlenk techniques. Solvents were dried and distilled under argon prior to use: toluene was dried over sodium, tetrahydrofuran (THF) was dried over sodium/benzophenone ketyl, and methylene chloride ($CH_2Cl_2$) was dried over phosphorus pentoxide ($P_2O_5$). Deuterated methylene chloride ($CD_2Cl_2$) and toluene-$d_8$ were purchased from Cambridge Isoptope Laboratories Inc. in 1 g ampules and used as received. All reagents were purchased from Aldrich and used as received. IR spectra were collected using a Nicolet 510-FTIR spectrometer at ambient temperature. EPR spectra were recorded on an X-band (9.8 GHz) Brüker EMX EPR spectrometer. Chemical ionization (CI) mass spectra were obtained at the University of Waterloo Mass Spectrometry Facility, Waterloo, ON, Canada, on a JEOL HX110 double-focusing mass spectrometer. Elemental analyses were performed by MHW laboratories, Phoenix, AZ. Copper(II) and manganese(II) bis(hexafluoroacetylacetonate) dihydrate M(hfac)$_2$·2H$_2$O (M = Cu, Mn) were prepared following the literature method[11] and prior to use were dehydrated by recrystallization in warm THF to yield the respective etherates M(hfac)$_2$·2THF (M = Cu, Mn); absence of hydrate peak at ca. 3410 cm$^{-1}$ in IR (KBr). The dithiadiazolyl radical ligand **1** and cobalt complex **4** were prepared according to literature procedures.[9] Sublimations were carried out in a three-stage variable temperature tube furnace.

**Synthesis of Mn Complex 2.** The dark red solution resulting from the addition of 10 mL of THF to a solid mixture of Mn(hfac)$_2$·2THF (0.6342 g, 1.034 mmol) and **1** (0.1887 g, 1.036 mmol) was stirred for 0.5 h with gentle warming. The solvent was removed in vacuo to afford **2** as a dark red powder, which was then purified by sublimation (125 °C for 18 h) under dynamic vacuum ($10^{-2}$ Torr) to yield dark red shiny blocks, 0.500 g (0.768 mmol, 74%). Red needles of **2** suitable for X-ray crystallography were grown by slow sublimation (120 °C for 5 d) under static vacuum ($10^{-2}$ Torr). IR (KBr): 1647 (vs), 1603 (w), 1555 (m), 1528 (s), 1504 (s), 1399 (m), 1321 (vw), 1258 (vs), 1197 (vs), 1149 (vs), 1099 (s), 1050 (w), 1016 (w), 949 (w), 921 (w), 855 (w), 795 (s), 766 (w), 751 (w), 742 (w), 665 (s), 655 (m), 638 (w), 585 (m), 524 (m), 472 (vw), 412 (w) cm$^{-1}$. Mass spectra (CI $NH_3$(g), $5 \times 10^{-6}$ Torr, 200 eV, 200 °C): *m*/*z* 669 $(M^+ + NH_4)^+$ 2%, 626 $(M^+ - C_2H)^+$, 548 $([M^+ + H] - CN_2S_2)^+$, 461 $([M^+ + NH_3] - C_5HO_2F_6)^+$ 100%, 444 $(M^+ - C_5HO_2F_6)^+$, 218, 200 $(C_6H_4N_3S_2^+ + NH_4)^+$, 183 $(C_6H_4N_3S_2^+ + H)^+$ 75%, 122 $([C_6H_4N_2^+ + NH_4] - NS_2)^+$, 105 $(C_6N_2H_4^+ + H)^+$, 78 $(C_5H_4N)^+$. Anal. Calcd. for $MNC_{16}H_6N_3S_2O_4F_{12}$: C, 29.51; H, 0.93; N, 6.45%. Found: C, 29.76; H, 0.84; N, 6.47%.

**Synthesis of Cu Complex 3.** The black solution resulting from the addition of 10 mL of $CH_2Cl_2$ to a solid mixture of Cu(hfac)$_2$·2THF (0.3740 g, 0.6014 mmol) and **1** (0.1090 g, 0.5981 mmol) was stirred for 0.5 h at ambient temperature. The solvent was then removed in vacuo to afford **3** as a dark brown powder; crude yield 0.3600 g (0.5455 mmol, 91.12%). Shiny black blocks of **3** suitable for X-ray crystallography and elemental analysis were grown by slow evaporation of $CH_2Cl_2$ at −25 °C from a saturated solution under argon atmosphere; yield 0.28 g (0.42 mmol, 70%). IR (KBr): 3137 (w), 3108 (w), 1656 (vs), 1642 (vs), 1607 (m), 1557 (s), 1533 (vs), 1476 (vs), 1425 (s), 1340 (m), 1260 (vs), 1205 (vs), 1147 (vs), 1085 (s), 1051 (m), 1028 (m), 945 (w), 929 (w), 884 (m), 803 (s), 793 (s), 749 (m), 742 (m), 667 (s), 653 (m), 589 (m), 543 (m), 527 (m), 415 (vw) cm$^{-1}$. Anal. Calcd for $CuC_{16}H_6N_3S_2O_4F_{12}$: C, 29.12; H, 0.92; N, 6.37%. Found: C, 29.40; H, 0.79; N, 6.36%.

**Structure Determination of 2 and 3.** Details can be found in the Supporting Information.

**Solid-State Magnetic Measurements.** Solid-state magnetic susceptibilities for **2**−**4** were measured on a Quantum Design MPMS-XL7 SQUID magnetometer using an applied field of 1.8, 1.0, and 0.4 T, respectively. Appropriate fields were determined from the magnetization plots at 2 K. Microcrystalline samples were loaded into the sample space of a Delrin sample holder and mounted to the sample rod. Data were corrected for sample holder (subtraction of measured background) and molecular diamagnetism (Pascal's constants).

**Solution Magnetic Measurements.** Evans' method[12] was used to measure magnetic properties of **2**−**4** in solution with toluene and with $CD_2Cl_2$. Samples were prepared in Teflon-sealed NMR tubes under argon at ambient temperature. Using toluene as a solvent, solutions of known concentration (5.03, 4.89, and 6.44 mM for **2**, **3**, and **4**, respectively) were prepared under argon atmosphere at ambient temperature. Melting point tubes loaded with these solutions were flame-sealed under argon atmosphere and inserted into an NMR tube containing neat toluene-$d_8$. The difference in $^1$H chemical shift of the toluene methyl protons from the solution insert and the contaminant toluene in the toluene-$d_8$ reference was used to calculate magnetic susceptibilities. Changes in the density of toluene (and hence the concentration of the solutions) with temperature were accounted for by using the Rackett equation.[13] In the case of $CD_2Cl_2$ solution measurements, neat $CD_2Cl_2$ with

(8) (a) Oakley, R. T. *Prog. Inorg. Chem.* **1988**, *36*, 299 and references therein. (b) Rawson, J. M.; Banister, A. J.; Lavender I. *Adv. Mater. Chem.* **1995**, *62*, 137 and references therein. (c) Rawson, J. M.; Alberola, A.; Whalley, A. *J. Mater. Chem.* **2006**, *16*, 2560 and references therein.
(9) Hearns, N. G. R.; Preuss, K. E.; Richardson, J. F.; Bin-Salamon, S. *J. Am. Chem. Soc.* **2004**, *126*, 9942.
(10) Jennings, M.; Preuss, K. E.; Wu, J. *Chem. Commun.* **2006**, 341.
(11) Izumi, F.; Kurosawa, R.; Kawamoto, H.; Akaiwa, H. *Bull. Chem. Soc. Jpn.* **1975**, *48* (11), 3188.
(12) Evans, D. F. *J. Chem. Soc.* **1959**, 2003.
(13) Lide, D. R., Kehiaian, H. V., Eds. *CRC Handbook of Thermophysical and Thermochemical Data*; CRC Press: Boca Raton, FL, 1994; p 81.

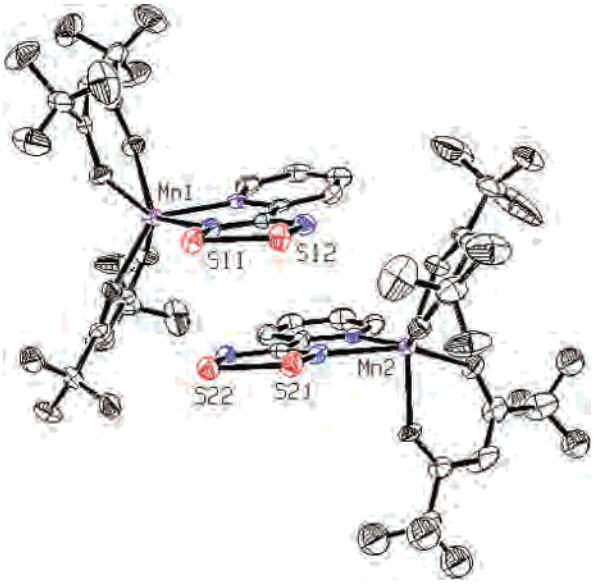


**Figure 1.** ORTEP representation of a dimer of **2**.

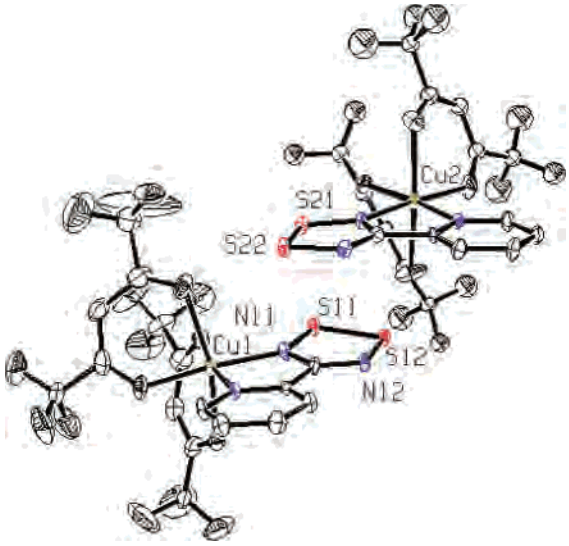


**Figure 2.** ORTEP representation of a dimer of **3**.

tetramethylsilane (TMS) flame sealed in a melting point tube was used as an internal reference insert inside each NMR tube containing a known concentration of sample in $CD_2Cl_2$ (0.0461, 0.0111, and 0.328 g/mL at ambient temperature for **2**, **3**, and **4**, respectively). The TMS $^1$H chemical shift was monitored. To account for the changes in solvent density with temperature, we used the Rackett equation for $CH_2Cl_2$.[13] $^1$H NMR spectra were recorded on a Brüker Avance-400 spectrometer with bbi probe (400 MHz for $^1$H) from 298 to 180 K, except in the case of the $CD_2Cl_2$ measurement of **4**, which was recorded on a Brüker Avance-300 with bbo probe (300 MHz for $^1$H) at the University of Waterloo. Molecular and solvent diamagnetic corrections were applied using Pascal's constants. Temperature readings from the internal thermocouple were calibrated using a glass/Hg thermometer in the spectrometer cavity.

**Cyclic Voltammetry.** Electrochemical measurements were collected on an Autolab PGSTAT30 in anhydrous $CH_2Cl_2$ at ambient temperature with 0.05 M $n$Bu$_4$PF$_6$ as supporting electrolyte and substrate concentrations of ca. 2.0 mM. A three-electrode glass cell sealed under argon atmosphere was used with platinum wire for all three electrodes (working, reference, and counter). The ferrocene/ferrocenium couple ($E_{1/2}$ = 0.48 V vs SCE under the same conditions)[14] was employed as an internal reference.

**Variable Temperature UV−Vis Absorption Spectroscopy.** Solutions of **1**−**4** were prepared under argon atmosphere in anhydrous toluene: 5.49, 4.21, 4.12, and 1.34 mM, respectively, at ambient temperature. UV−visible absorption data were collected on a Varian Cary5E spectrophotometer. A Specac 4000 series high stability temperature controller (accurate to ± 0.1 K) with NaCl windows was used for the variable temperature data collection. Changes in solvent density with temperature were accounted for by using the Rackett equation.[13]

## Results

**Crystal Structures.** The single-crystal X-ray structures of complexes **2** (Figure 1) and **3** (Figure 2) confirm the bidentate chelation of ligand **1** to the metal center via the pyridine nitrogen atom and one of the DTDA nitrogen atoms. For both complexes, there are two molecules in the asymmetric unit. Both of the crystallographically distinct molecules of both complexes have several features in common. In all cases, the pyridine ring and DTDA ring of the coordinated ligand are roughly coplanar, with a dihedral N−C−C−N angle ranging from ca. +0.8° to −2.7°. This is, in fact, a smaller dihedral angle than that observed for either the cobalt complex **4** (−7.8(6)°) or the free ligand **1** (−3.7(3)° and −11.5(4)° for the two molecules in the asymmetric unit.)[9] It should be noted, however, that in complex **2** the DTDA ligand is somewhat bowed such that there is a slight curvature along its long axis.

The intramolecular S−S (bond) distance in the DTDA ring ranges from 2.087(3) to 2.093(3) Å for complexes **2** and **3**. This is comparable to the intramolecular S−S distance in the free ligand **1** (2.0935(10) Å; dimerized in the solid state) and in the cobalt complex **4** (2.089(2) Å; not dimerized in the solid state.) This distance has been shown to give a reliable indication of the oxidation state of DTDA rings since the singly occupied molecular orbital (SOMO) of the neutral radical is a $\pi^*$ orbital that is antibonding with respect to the S−S bond. A one-electron oxidation of the DTDA ring to a closed shell cation is typically accompanied by a significant shortening of the S−S distance.[15]

Inspection of the crystal structure of the manganese complex **2** reveals different coordination geometries about the metal atom for the two crystallographically distinct molecules. While one molecule appears to have pseudo-trigonal symmetry about the Mn1 atom, reminiscent of other known Mn$^{II}$ complexes,[16] the site symmetry about atom Mn2 in the other molecule is quite distorted and qualifies neither as pseudo-trigonal nor pseudo-octahedral. In comparison, the site symmetry about atoms Cu1 and Cu2 (the copper atoms in the two crystallographically distinct molecules) appears to be pseudo-octahedral with an elongation along an axis

(14) Boeré, R. T.; Roemmele, T. L. *Coord. Chem. Rev.* **2000**, *210*, 369.

(15) (a) Ruangsuttinarupap, S.; Gross, H.-D.; Willing, W.; Müller, U.; Dehnicke, K *Z. Anorg. Allg. Chem.* **1986**, *536*, 153. (b) Hazell, A.; Hazell, R. G. *Acta Crystallogr. C* **1988**, *44*, 1807.

(16) van Gorkum, R.; Buda, F.; Kooijman, H.; Spek, A. L.; Bouwman, E.; Reedijk, J. *Eur. J. Inorg. Chem.* **2005**, 2255.

perpendicular to the plane of the DTDA ligand, indicating a pseudo-Jahn−Teller distortion typical of a $d^9$ metal complex. The metal site symmetry in the cobalt complex **4** was shown to be pseudo-octahedral with no significant distortions.[9]

In stark contrast to complex **4**, which crystallizes with no significant interaction between the DTDA rings of neighboring molecules, complexes **2** and **3** both exhibit short intermolecular contacts between heteroatoms in the solid state. Furthermore, the mode of interaction in complex **2** is different from that in complex **3**.

In the manganese complex **2**, neighboring molecules crystallize as dimers via $\pi$-stacking of the DTDA ligands. The orientation of the molecules is such that the DTDA rings are eclipsed and two short intermolecular S···S contacts are established. This type of dimer conformation has been referred to as a *cis*-cofacial dimerization and is typical of DTDA radicals of the type R-$CN_2S_2$ where R is an aromatic ring.[17] At 100 K, the S11···S22 distance is 3.043 Å and the S12···S21 distance is 2.995 Å. This is within the sum of van der Waals radii for sulfur atoms (3.6 Å) and is reminiscent of the dimerization observed in the solid state for the free ligand **1**.[9]

In the copper complex **3**, neighboring molecules form dimer pairs through $\pi$-stacking, but the orientation of the molecules is such that the cofacial DTDA rings are rotated approximately 90° with respect to one another about an axis through the ring centroids, R = $N(CH_3)_2$. The short intermolecular contact S11···S12 is 2.948 Å at 100 K. This dimer orientation has been referred to as *twisted*-cofacial dimerization and has been observed in the solid-state packing of DTDA radicals of the type R-$CN_2S_2$ where steric interaction between nonplanar R groups prevents the *cis*-cofacial dimerization mode (e.g., for R = $CF_3$,[18] Me,[19] and $NMe_2$).[20]

**Magnetic Measurements.** The temperature-dependent magnetic susceptibilities of **2** and **3** were measured both in the solid state and as solutions in $CD_2Cl_2$ and toluene. The results of these measurements are presented in Figure 3 as $\chi T$ vs $T$ plots, where $\chi$ is the paramagnetic susceptibility. Although the solid-state magnetic susceptibility of **4** has been reported previously,[9] it is also included here along with the previously unreported $CD_2Cl_2$ and toluene solution measurements for comparison.

For **2** as a microcrystalline solid, the $\chi T$ value at room temperature is 4.2 emu K $mol^{-1}$, close to the expected value of 4.377 for one isolated $S = 5/2$ spin center (assuming $g = 2$). Upon cooling, $\chi T$ remains relatively constant until, at approximately 50 K, it starts to decrease. A Curie−Weiss fit of the measured data, shown in Figure 3, gives values of $g = 1.996$ and $\theta = -2.4$ K. This result indicates the absence of measurable spin on the DTDA ligand owing to dimerization observed in the solid state. A negative Weiss constant implies a weak antiferromagnetic intermolecular interaction, presumably between the two manganese centers of a dimer pair, mediated through the close contacts of the DTDA ligands. Using the definition $\theta = zJS(S + 1)/3k$, where $z$ is the number of nearest neighbors around a given magnetic molecule in a crystal lattice (equal to 1 for the dimer) and $k$ is the Boltzmann constant, the intra-dimer exchange parameter $J$ is calculated to be $-0.29$ $cm^{-1}$.

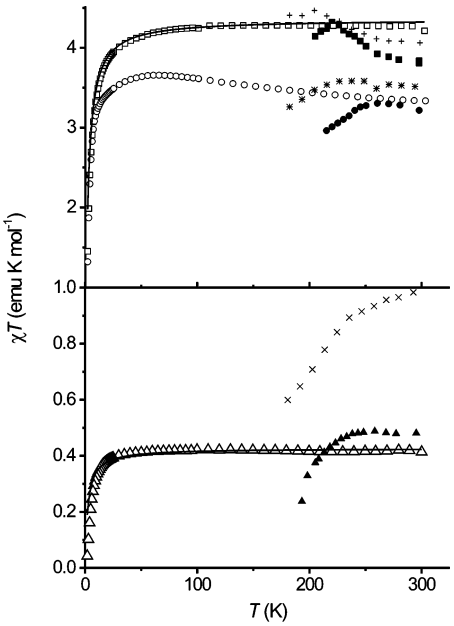


**Figure 3.** Measured $\chi T$ vs $T$ data for complex **2** in the solid state (□), in $CD_2Cl_2$ (■), and in toluene (+); for complex **3** in the solid state (△), in $CD_2Cl_2$ (▲), and in toluene (×); and for complex **4** in the solid state (○), in $CD_2Cl_2$ (●), and in toluene (∗). The solid-state data for **2** and **3** were modeled using a Curie−Weiss fit (−).

The magnetic susceptibility measurements of **3** in the microcrystalline solid-state suggest a similar scenario. The room temperature $\chi T$ value is 0.42 emu K $mol^{-1}$. This is close to the expected value of 0.375 for an isolated $S = 1/2$ spin center ($g = 2$). The value of $\chi T$ remains roughly constant with decreasing temperature until 50 K where it starts to decrease. The measured data was fit (Figure 3) to the Curie−Weiss equation with values of $g = 2.1322$ and $\theta = -2.5$. This result is consistent with the loss of spin on the DTDA ligands in the solid state through the formation of dimers. The negative Weiss constant is indicative of a weak antiferromagnetic intermolecular interaction. As with **2**, it is suggested that this interaction is between the copper centers of a dimer pair and mediated through the short contacts between DTDA ligands. As calculated from the Weiss constant, the intra-dimer exchange parameter is $J = -3.5$ $cm^{-1}$.

Given that, in the solid state, the DTDA ligand dimer is effectively rendered diamagnetic, we have measured the magnetic susceptibilities of **2** and **3** as solutions in toluene and $CD_2Cl_2$ using Evans' method.[12] This experiment was performed in order to probe the magnetic properties of the individual monomeric molecules. We have determined the monomer/dimer equilibria as a function of temperature in toluene to better ascertain which species is contributing to

(17) Vegas, A.; Pérez-Salazar, A.; Banister, A. J.; Hey, R. G. *J. Chem. Soc. Dalton Trans.* **1980**, 1812.
(18) Hofs, H.-U.; Bats, J. W.; Gleiter, R.; Hartmann, G.; Mews, R.; Eckert-Maksić, M.; Oberhammer, H.; Sheldrick, G. M. *Chem. Ber.* **1985**, *118*, 3781.
(19) Banister, A. J.; Hansford, M. I.; Hauptmann, Z. V.; Wait, S. T.; Clegg, W. J. *J. Chem. Soc. Dalton Trans.* **1989**, 1812.
(20) Cordes, A. W.; Goddard, J. D.; Oakley, R. T.; Westwood, N. P. C. *J. Am. Chem. Soc.* **1989**, *111*, 6147.

the measured magnetic susceptibility (see following sections.) We have also measured the variable temperature solution magnetic susceptibility of **4** for comparison. It should be noted that the solutions were prepared by weighing solute and solvent (±0.0001 g accuracy) and the accuracy in temperature measurement is ca. ± 0.2 K. Thus, the error bars on the reported solution $\chi T$ values are ≤10%.

In the case of complex **2**, the $\chi T$ value in solution is lower than that in the solid state at room temperature (3.8 emu K mol$^{-1}$ in $CD_2Cl_2$; 4.06 emu K mol$^{-1}$ in toluene). As the temperature is decreased, the value of $\chi T$ increases until it reaches a maximum value (4.3 emu K mol$^{-1}$ at 220 K in $CD_2Cl_2$; 4.46 emu K mol$^{-1}$ at 200 K in toluene). This is roughly the same as the measured value in the solid state. As the temperature is lowered further, the $\chi T$ value begins to decrease again. In contrast, the solution $\chi T$ value for **3** at room temperature is higher than that measured in the solid state (0.48 emu K mol$^{-1}$ in $CD_2Cl_2$; 0.98 emu K mol$^{-1}$ in toluene). As the temperature is lowered, the value of $\chi T$ eventually decreases. In $CD_2Cl_2$, the value actually drops below the solid-state value at ca. 210 K. Finally, the solution value of $\chi T$ for **4** at room temperature is roughly the same as the solid-state value in both toluene and $CD_2Cl_2$. Upon cooling, the solution $\chi T$ value remains identical to the solid-state value until, at ca. 240 K in $CD_2Cl_2$ and at ca. 210 K in toluene, it starts to decrease, deviating from the solid-state value. The measurements were all performed with decreasing temperature. For all $CD_2Cl_2$ solutions, precipitation was observed at the lowest measured temperatures. No precipitation was observed in toluene.

**TD-DFT Calculation.** We speculated that the solution magnetometry measurements could be readily explained given that a temperature-dependent monomer/dimer equilibrium exists in solution. We have observed the development of an intense orange-red color when dilute (essentially colorless at ambient temperature) solutions of **1**−**4** are cooled by immersion of a vessel in liquid nitrogen. We hypothesized that this absorption may be related to the formation of dimers in solution. In order to ascertain whether this was a plausible assumption, we employed time dependent density functional theory (td (u)b3lyp/6-31++g(d,p) with scf = tight, as found in the Gaussian 03W computational software)[21] to calculate the oscillator energies and strengths in the visible region for the gas-phase monomer of the free ligand **1** and the gas-phase dimer of **1**. We used the crystal structure geometries without optimization in both cases, and we set the ground state of the dimer to a closed shell singlet (i.e., diamagnetic). We used the SWizard program[22] in order to generate the spectral representations of the calculation results from the Gaussian output. These calculations predict a very intense absorption at ca. 450 nm (2.744 eV) in the dimer that is absent in the monomer (Figure 4). This absorption arises primarily from an excitation from the dimer HOMO (orbital 93) to the dimer LUMO (orbital 94), both of which have (virtual) electron density primarily on the sulfur and nitrogen atoms (Figure 5).

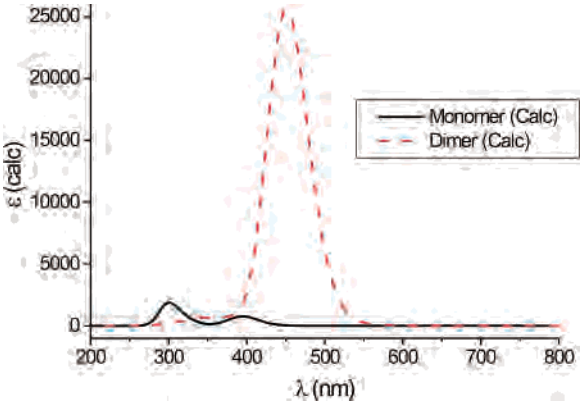


**Figure 4.** Visible absorption spectra of the monomer and dimer of **1** as calculated using TD−DFT. Plots generated using Swizard.[22]

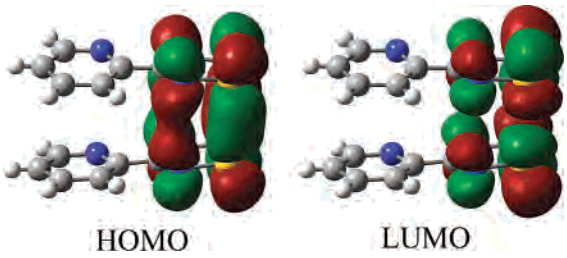


**Figure 5.** Ligand dimer HOMO and ligand dimer LUMO, generated using GaussView 3.0; surface isovalue = 0.02.

**Absorption Spectroscopy.** The above computational evidence suggests that the intense orange-red color observed upon cooling a solution of **1** in various solvents ($CH_2Cl_2$, $CHCl_3$, toluene) is associated with the onset of dimerization. We assume that similar absorptions in the complexes have a similar origin and that measurement of the visible absorption spectra as a function of temperature for the free ligand **1** and for the complexes **2**−**4** in solution gives information on the monomer−dimer equilibria. In each case, we measured the spectrum as a function of temperature in toluene in a sealed cell. We derived the temperature dependence of an equilibrium constant $K_{eq}$ that describes the monomer−dimer equilibrium as follows:

$$2M \overset{K_{eq}}{\rightleftharpoons} D \qquad K_{eq} = [D]/[M]^2 \tag{1}$$

where $[D]$ and $[M]$ are the equilibrium concentrations of the dimer and monomer, respectively. This is a concept that has

(21) Frisch, M. J.; Trucks, G. W.; Schlegel, H. B.; Scuseria, G. E.; Robb, M. A.; Cheeseman, J. R.; Montgomery, J. A., Jr.; Vreven, T.; Kudin, K. N.; Burant, J. C.; Millam, J. M.; Iyengar, S. S.; Tomasi, J.; Barone, V.; Mennuci, B.; Cossi, M.; Scalmani, G.; Rega, N.; Petersson, G. A.; Nakatsuji, H.; Hada, M.; Ehara, M.; Toyota, K.; Fukuda, R.; Hasegawa, J.; Ishida, M.; Nakajima, T.; Honda, Y.; Kitao, O.; Nakai, H.; Klene, M.; Li, X.; Knox, J. E.; Hratchian, H. P.; Cross, J. B.; Adamo, C.; Jaramillo, J.; Gomperts, R.; Stratmann, R. E.; Yazyev, O.; Austin, A. J.; Cammi, R.; Pomelli, C.; Ochterski, J. W.; Ayala, P. Y.; Morokuma, K.; Voth, G. A.; Salvador, P.; Dannenberg, J. J.; Zakrzewski, V. G.; Dapprich, S.; Daniels, A. D.; Strain, M. C.; Farkas, O.; Malick, D. K.; Rabuck, A. D.; Raghavachari, K.; Foresman, J. B.; Ortiz, J. V.; Cui, Q.; Baboul, A. G.; Clifford, S.; Cioslowski, J.; Stefanov, B. B.; Liu, G.; Liashenko, A.; Piskorz, P.; Komaromi, I.; Martin, R. L.; Fox, D. J.; Keith, T.; Al-Laham, M. A.; Peng, C. Y.; Nanayakkara, A.; Challacombe, M.; Gill, P. M. W.; Johnson, B.; Chen, W.; Wong, M. W.; Gonzalez, C.; Pople, J. A. *Gaussian 03*, Revision B.03; Gaussian, Inc.: Pittsburgh, PA, 2003.

(22) Gorelsky, S. I. *SWizard*; Department of Chemistry, York University: Toronto, ON, 1999; http://www.sg-chem.net.

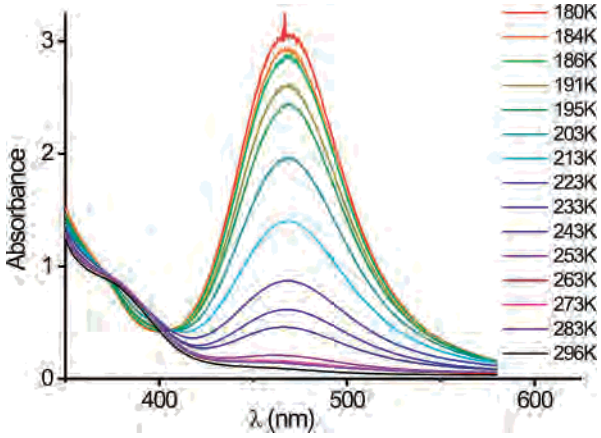


**Figure 6.** Absorption spectrum of **3** in toluene (4.12 mM at 23 °C) as a function of temperature.

been used to monitor the monomer−dimer equilibria of copper complexes to great effect.[23]

For the free ligand **1** and for all three complexes **2**−**4**, little or no absorption was recorded for toluene solutions (millimolar concentrations) at ca. 450 nm at room temperature. An absorption in this spectral region was observed to have increasing intensity upon cooling in all cases. The measured absorption as a function of temperature is shown for the copper complex **3** in Figure 6 as an example. Spectra for the other species can be found in the Supporting Information. For the free ligand **1**, the absorption is centered at 478 nm. For complexes **2**−**4**, it is centered at 455, 468, and 480 nm, respectively.

For each species, the observed extinction coefficient ($\epsilon_{obs}$) was calculated from the measured maximum absorbance at the wavelengths quoted above and from the solution concentration $[M]_o$ as calculated from initial quantities of solute and solvent at ambient temperature; $[M]_o$ adjusted for temperature-dependent solvent density changes[24] (cell path length of 0.1 cm). The $\epsilon_{obs}$ was then plotted as a function of inverse temperature (Figure 7) and fit with eq 2:[23]

$$\epsilon_{obs} = \left[\frac{\sqrt{1 + 8[M]_o \exp((\Delta S°/R) - (\Delta H°/RT))} - 1}{4[M]_o \exp((\Delta S°/R) - (\Delta H°/RT))} * \left(\epsilon_M - \frac{\epsilon_D}{2}\right)\right] + \frac{\epsilon_D}{2} \quad (2)$$

where $\epsilon_M$ is the extinction coefficient for the monomer; $\epsilon_D$ is the extinction coefficient for the dimer; and $\Delta S°$, $\Delta H°$, and $R$ have their usual meanings. Changes in the total concentration $[M]_o$ as a function of solvent density variation with temperature were explicitly accounted for using known density−temperature equations for toluene.[24] Fitting parameters for all four species are listed in Table 1, and plots of log $K_{eq}$ as a function of temperature are shown in Figure 8.

(23) (a) Lange, J.; Elias, H.; Paulus, H. *Inorg. Chem.* **2000**, *39*, 3342. (b) Maizlish, V. E.; Shirokov, A. V.; Kudrik, E. V.; Shaposhnikov, G. P. *Russ. J. Gen. Chem.* **2002**, *72* (10), 1640.

(24) Brunel, R. F.; Van Bibber, K. Density and thermal expansion of liquid organic compounds under atmospheric pressure. In *International Critical Tables, Vol. III*; Washburn, E. W., Ed.; Published for National Research Council by McGraw-Hill: New York, 1929; p 27.

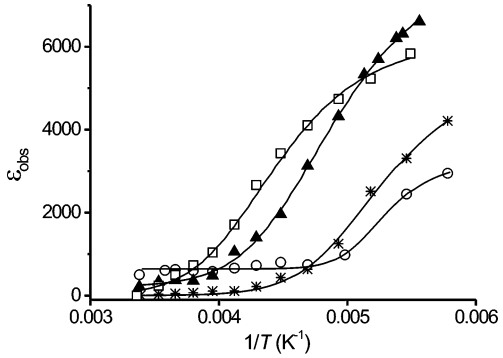


**Figure 7.** Observed extinction coefficients plotted as a function of inverse temperature for toluene solutions of ligand **1** (∗), Mn complex **2** (□), Cu complex **3** (▲), and Co complex **4** (○) and best fits (—) from eq 2.

**Table 1.** Best Fitting Parameters for Eq 2 for Toluene Solutions

| compound | $\Delta S°/R$ | $\Delta H°/R$ (in K) | $\epsilon_M$ | $\epsilon_D$ |
|---|---|---|---|---|
| **1** | −17.4 ± 1.1 | −4273 ± 243 | 0 (fixed) | 10586 ± 600 |
| **2** | −13.08 ± 0.74 | −4185 ± 189 | 0 (fixed) | 12314 ± 330 |
| **3** | −13.45 ± 0.72 | −3863 ± 164 | 210 ± 54 | 15972 ± 462 |
| **4** | −33.5 ± 2.3 | −7571 ± 484 | 641 ± 30 | 6443 ± 363 |

These results indicate that the monomer−dimer equilibrium constants for toluene solutions of **2** and of **3** are near unity at room temperature and shift in favor of the dimer at lower temperatures. Conversely, this equilibrium lies heavily in favor of the monomer in a toluene solution of the Co complex **4** at room temperature and does not favor the dimer until temperatures below ca. 230 K. This is in keeping with the observation that complexes **2** and **3** form dimers in the crystalline solid state and that **4** does not.

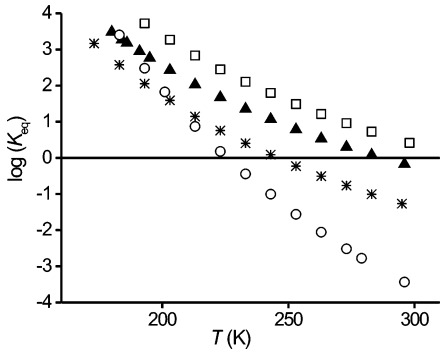


**Figure 8.** Variation of log $K_{eq}$ as a function of temperature for toluene solutions of ligand **1** (∗), Mn complex **2** (□), Cu complex **3** (▲), and Co complex **4** (○). The equilibrium constant is defined for 2 monomers to 1 dimer, such that values of log $K_{eq}$ < 0 arise for equilibria favoring the monomers.

**Electron Paramagnetic Resonance.** We have previously reported the room temperature EPR spectrum of the ligand **1** in $CH_2Cl_2$.[9] The spectrum of **1** in toluene at room temperature is similar, with a 1:2:3:2:1 five-line pattern indicating coupling of the unpaired electron to two approximately equivalent nitrogen atoms ($a_N$ = 5.18 G; $g$ = 2.010).[25] In an effort to probe the nature of the spin

(25) Simulation of measured EPR spectra were performed using the Winsim2002 software package provide by NIEHS/NIH Public EPR Software Tools (P.E.S.T.) (O'Brien, D. A.; Duling, D. R.; Fann, Y. C. 2002).

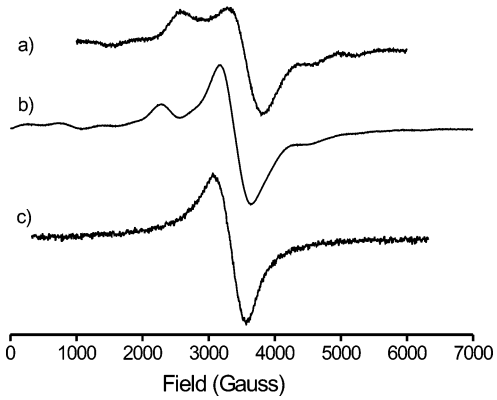


**Figure 9.** X-band EPR spectra of manganese complex **2**: (a) at room temperature in a microcrystalline solid state, (b) crystallized in toluene glass at 185 K, and (c) toluene solution at room temperature. MW frequency = 9.7292, 9.3467, and 9.3460 GHz, respectively.

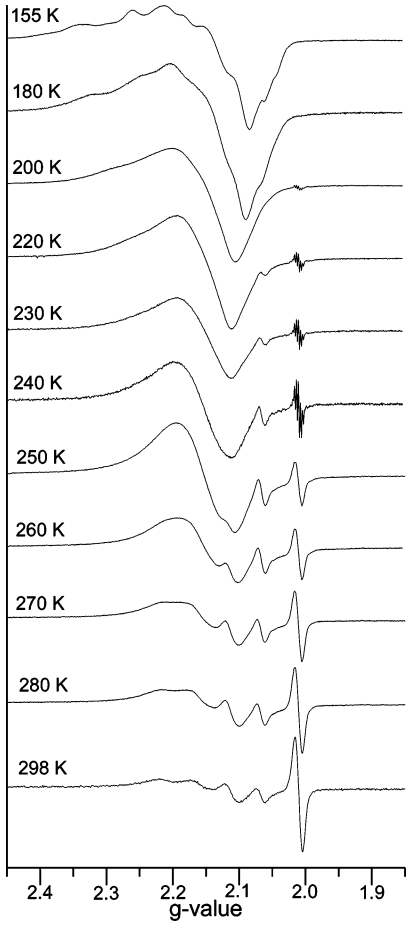


**Figure 10.** X-band EPR spectra of **3** in toluene at various temperatures. The instrument parameters have been optimized at each temperature in order to maximize the resolution. The spectra are plotted to maximize peak area in order to be legible, thus there is no meaning in the relative peak areas from plot to plot.

distributions in the metal complexes, we have measured the X-band EPR spectra of both the manganese complex **2** (Figure 9) and the copper complex **3** (Figure 10) over a range of temperatures in toluene and at room temperature in the solid state. These EPR spectra are difficult to analyze, primarily because of the monomer/dimer equilibrium issue. Both the monomer and the dimer may contribute to a given spectrum with the dimer becoming a greater contributor at lower temperature. At higher temperatures, where the monomer is favored in solution, the thermal energy ($kT$) available to the system is likely to be greater than the exchange energy ($J$), and thermal population of excited spin states may occur. Thus, we cannot expect to acquire spectra that elucidate the spin ground state of the monomer at higher temperatures, and at lower temperatures we can expect strong contributions from the dimer. A further technical detail is the difference in line widths between ligand-centered absorptions (narrow) and metal-centered absorptions (broad) owing to significant dipolar interactions (usually described by constants $D$ and $E$) for the metal nuclei. Thus, the optimal instrument parameters and solution concentrations may be different for different regions of the spectra.

A few general remarks can be made regarding the expected appearance of the EPR spectra of the monomers. We can treat a spectrum as the superposition of the radical DTDA and metal ion species if the exchange energy ($J$) is small as compared to the difference in the $g$-values between the free ligand **1** and the parent metal complex ($\Delta g$) and compared to the electron-nuclei hyperfine coupling constants.[26] If $J$ is larger than $\Delta g$, then the center of the EPR spectrum ($g_{\text{eff}}$) of the complex will be between the centers of the spectra of **1** and of the parent metal complex. If $J$ is large compared to the hyperfine coupling to $^{14}$N on **1** and the metal nucleus, then all unpaired electrons will be coupled to both nuclei. Finally, in species with integer spin values ($S = 1, 2, 3, ...$), it is sometimes the case that zero-field splitting is large enough to remove the degeneracy of the microstates to such a degree that an EPR spectrum is not observed in the X-band.

Toluene solution measurements of **2** at room temperature reveal one broad absorption centered at $g = 2.02$. The spectrum is similar in appearance to typical X-band EPR spectra of $^{55}Mn^{2+}$ species in solution.[27] According to the thermodynamic data, a significant percentage of the complex in solution is involved in dimer formation, even at room temperature. The spin ground state of the dimer is $S = 0$ owing to AFM coupling between two complexes. This may render the $(DTDA)_2$ component of the dimer diamagnetic, but the exchange coupling between the two $d^5$ metal ions is small ($J_{Mn-Mn} \ll kT$) so thermal population of excited spin states occurs at room temperature, and we can treat the dimer contribution as the superposition of two $^{55}Mn^{2+}$ species. The spin ground state of the monomeric complex is either $S = 2$ or 3 (AFM or FM coupling of the $d^5$ ion to the paramagnetic ligand). The solution magnetometry suggests that thermal population of excited spin states occurs at room temperature, and these may also contribute to the spectrum. Nevertheless, the broad line width of the observed spectrum masks any hyperfine coupling that may or may not be present.

We have collected EPR spectra of toluene solutions of **2** at three different concentrations (112, 15.09, and 1.45 mM),

(26) Richardson, P. F.; Kreilick, R. W. *J. Magn. Res.* **1978**, *29*, 285.
(27) (a) Burlamacchi, L.; Martini, G.; Ottaviani, M. F.; Romanelli, M. *Adv. Mol. Relax. Interact. Proc.* **1978**, *12*, 145. (b) Poupko, R.; Luz, Z. *Mol. Phys.* **1978**, *36* (3), 733. (c) Mazur, M.; Kleinova, M.; Moncol, J.; Stachova, P.; Valko, M.; Telser, J. *J. Non-Cryst. Solids* **2006**, *352*, 3158.

cooling from room temperature. In all cases, we observe the same phenomenon. There is no change in the spectrum as described above at any temperature at which the complex is dissolved in the toluene, either liquid or glass. For the most concentrated solution, a sludge of precipitated complex forms near the melting point of toluene, and for the 15.09 mM solution, crystalline needles of **2** form at 155−158 K in the toluene glass. In both cases, the precipitation of the complex is accompanied by the onset of new absorptions in the EPR spectrum, closely resembling the microcrystalline solid-state spectrum discussed below. No precipitate was observed upon cooling the least concentrated solution and no change in the spectrum was observed over the measured temperature range (298−150 K).

In the solid state, a more complex spectrum is observed for **2** than is observed in solution. The dominant feature is a broad absorption centered at $g_{eff} = 1.98$. There are also features present at lower and higher field, notably a smaller broad absorption centered at $g_{eff} = 2.55$ in the microcrystalline sample at room temperature and at $g_{eff} = 2.75$ in the solid precipitate from toluene (low temperature). It has been suggested that an $Mn^{II}L_6$ complex with regular octahedral symmetry should have a single line at $g_{eff} \approx 2$ and that zero-field splitting arising from geometrical distortions, or the presence of more than one type of ligand, will split this line generating lower and higher field components.[28] The solid-state X-band EPR spectrum of $Mn(NCS)_6^{4-}$, for example, gives a broad absorption at $g_{eff} \approx 2$ with a relatively symmetric distribution of lower and higher field components.[28] The spectrum of $[Mn(^9aneN_3)_2](ClO_4)_2$ is significantly less symmetric in appearance, with $g_{eff} = 1.98$ and large contributions from the axial and rhombic zero field-splitting parameters $D$ and $E$.[29] The powder X-band EPR spectrum of $Mn(acac)_2(bpy)$, which has pseudo-trigonal symmetry, has been reported recently and shows a strong nonisotropic resonance signal at $g_{eff} = 3.25$.[16] For complex **2**, there are two $Mn^{II}$ ions with different ligand sphere symmetries in the crystallographic unit cell, which increases the complexity of this spectrum and makes it very difficult to fit to a spin Hamiltonian with any measure of certainty. We have, therefore, refrained from fitting this spectrum, but there are a number observations that can be made nonetheless. The spectrum appears to resemble the spectra of $Mn(NCS)_6^{4-}$ and $[Mn(^9aneN_3)_2](ClO_4)_2$ more closely than that of $Mn(acac)_2(bpy)$. This includes the absence of a strong resonance signal at $g_{eff} \gg 2$. There is no evidence of hyperfine structure related to coupling with the $^{55}Mn$ nucleus, $^{14}N$ nuclei, or any other nuclei. The crystal structure of **2** confirms that the complexes form dimers in the solid state. Although weak coupling between the spins of the two manganese ions generates an $S = 0$ ground state, at room temperature excited spin states will be occupied and it is more appropriate to treat this system as two independent $Mn^{2+}$ ions. The dimerization does, however, couple the DTDA spins very strongly antiferromagnetically such that no ligand-based EPR absorption is observed. It should be noted that crystal packing is never perfect; therefore, we might expect a small percentage of the complex to remain undimerized in the solid state, although we have detected no evidence for this. It should also be noted that a recent report has shown that the solid-state EPR spectrum of dimers of radical thiazyls shows a contribution from an $S = 1$ excited state that is thermally populated at room temperature.[30] There is no evidence of a similar excited-state contribution involving the DTDA ligands of the dimers of complex **2**.

In contrast to the manganese complex **2**, the EPR spectrum of the copper complex **3** in toluene (16 mM) changes dramatically with decreasing temperature. No precipitate was observed over the measured temperature range of 298−155 K. The room temperature spectrum appears to have two components; a sharp absorption at $g = 2.010$ and, at lower field, the broad four-line pattern typical of an isotropic solution spectrum with hyperfine coupling to one $^{63/65}Cu$ nucleus ($g_{eff} = 2.14$). A significant percentage of the complex in solution at ambient temperature is involved in dimer formation at concentrations required for the observation of an EPR spectrum, according to the equilibrium data established by visible absorption spectroscopy. The spin ground state of the dimer is expected to be $S = 0$ owing to AFM coupling. The coupling between the DTDA spins is expected to be significant, making the $(DTDA)_2$ component of the dimer effectively diamagnetic. However, the coupling between the two copper ions of the dimer is weak ($J_{Cu-Cu} \ll kT$ at RT) and we can reasonably expect thermal population of excited spin states at RT such that we can treat the dimer contribution to the EPR spectrum as that of two independent $Cu^{2+}$ ions. The ground state spin of the monomer is $S = 0$ or 1 (for either AFM or FM coupling between the unpaired electron on the DTDA and that of the $d^9$ $Cu^{2+}$ ion.)

The broad four-line pattern ($g_{eff} = 2.14$) of the room temperature EPR spectrum arises from hyperfine coupling of an electron to the $^{63/65}Cu$ nucleus in either the monomer or the dimer, or may be the superposition of the two. The sharp absorption at $g = 2.010$ is a contribution from the unpaired electron on the DTDA ring. As the solution is cooled, the sharp absorption becomes a well-resolved 1:2:3:2:1 five-line pattern (coupling to two $^{14}N$ nuclei; $a_N \approx 5.0$ G)[25] similar to the spectrum of **1**. The explanation for the observation of a copper component plus a DTDA component in the spectrum may be that $J$ is small as compared to the difference in $g$-values of the metal and radical ligand components, which is relatively large. It can also be argued that the EPR spectrum shows the dissociation of the metal from the DTDA ligand. Although we have no direct evidence that this is not the case, there are a number of arguments that can be made against this second possibility. We have measured the EPR spectrum of $Cu(acac)_2 \cdot 2H_2O$ with an

(28) Dowsing, R. D.; Gibson, J. F.; Goodgame, D. M. L.; Goodgame, M.; Hayward, P. J. *Nature* **1968**, *219*, 1037.

(29) Gahan, L. R.; Grillo, V. A.; Hambley, T. W.; Hanson, G. R.; Hawkins, C. J.; Proudfoot, E. M.; Moubaraki, B.; Murray, K. S.; Wang, D. *Inorg. Chem.* **1996**, *35*, 1039.

(30) Cameron, T. S.; Decken, A.; Kowalczyk, R. M.; McInnes, E. J. L.; Passmore, J.; Rawson, J. M.; Shuvaev, K. V.; Thompson, L. K. *Chem. Commun.* **2006**, 2277.

insert containing the free ligand **1**. In order to obtain a spectrum with both the $Cu^{2+}$ and DTDA signals, we had to adjust the concentrations such that the [$Cu^{2+}$] in the cavity was 6 orders of magnitude higher than the [DTDA]. Furthermore, the visible absorption spectra as a function of temperature (in toluene) and cyclic voltammetry (in $CH_2Cl_2$) are significantly different for **1** as compared to **2**, suggesting that we are not observing dissociated ligand and metal components in our other solution experiments. Thus, we are confident that the bulk of the complex remains intact. This does not rule out a very small amount of metal−ligand dissociation. It can only be noted that these complexes can be sublimed under static vacuum, demonstrating that the coordination remains intact in the gas phase and that toluene is not a coordinating solvent and therefore the dissociation would not be favored in toluene any more than it would be in the gas phase.

As the solution is cooled from room temperature, the equilibrium shifts in favor of the dimer. Resolution of the broad four-line pattern is lost, but the sharp five-line pattern can be resolved between 240 and 200 K. Below 200 K, the five-line pattern is lost and a more complex spectrum is observed centered at $g_{eff} = 2.14$. This may be the onset of the resolution of the $g_{||}$ and $g_{\perp}$ components of the copper spectrum, perhaps complicated by hyperfine coupling of unpaired electrons to both copper nuclei of a dimer in the triplet excited state.

In the solid state at room temperature, the EPR of **3** appears as a broad unresolved singlet centered at $g = 2.10$-(3) with a small feature at lower field (see Supporting Information). No hyperfine coupling is resolved.

Other solution spectra of $Cu^{2+}$ radical ligand complexes have been reported in the literature.[27,31] These are typically performed at low temperature in order to resolve small hyperfine couplings and it has been observed that the nature of the solvent may greatly influence the appearance of the spectrum. We encounter issues to do with dimerization at low temperatures, so this avenue is not promising. We have also collected ambient temperature EPR spectra in methylene chloride and in chloroform (see Supporting Information), but in neither solvent can further coupling be observed.

**Cyclic Voltammetry.** In order to further probe the nature of these complexes, we have collected cyclic voltammetry (CV) measurements of **2**−**4** in $CH_2Cl_2$ with 0.05 M $n$Bu$_4$NPF$_6$ electrolyte (Figures 11−13). A sweep rate of 0.5 V/s is shown in all cases. In order to determine that the reported electron-transfer processes are indeed diffusion-controlled rather than surface-controlled at this scan rate, multiple cyclic voltammograms with sweep rates from 0.05 to 1.0 V/s were measured for species **2** and **4**, and plots of first oxidative peak current (and peak current for the reverse reduction of this process) versus the square root of the scan rate were evaluated. An excellent linear relationship was observed at the chosen sweep rate of 0.5 V/s for both processes in both species. We compare the results to CV measurements of the free ligand **1** and the M(hfac)$_2$(THF)$_2$ (M = Mn, Cu, Co) starting materials (see Supporting Information) under the same conditions. All potentials are quoted versus SCE. A summary of the redox processes is provided in Table 2.

When the applied potential is swept out to a maximum of ca. 2.5 V, the CV of the manganese complex **2** reveals two irreversible oxidation peaks at 1.24 and 2.17 V, respectively, with a very sharp reduction peak, with roughly twice the peak area, at 0.93 V on the return sweep. If, however, the applied potential is swept out to no more than 1.8 V, a reversible oxidation wave at $E_{1/2}(ox) = 1.16$ V is observed. We propose the following explanation of this phenomenon.

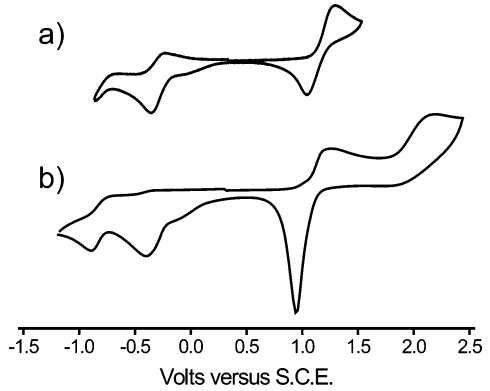


**Figure 11.** Cyclic voltammetry of **2** in $CH_2Cl_2$ with 0.05 M $n$Bu$_4$NPF$_6$ electrolyte; sweep rate of 0.5 V/s; oxidative direction swept first. (a) Potentials limited to ca. $-0.85 < V < 1.5$. (b) Potentials swept to ca. 2.5 and −1.25 V.

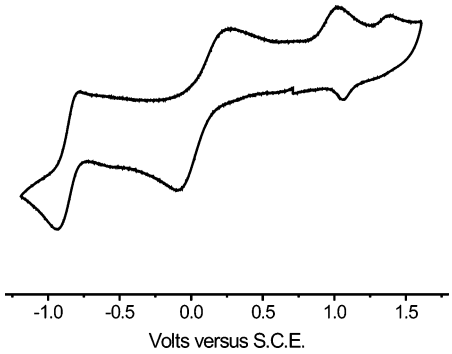


**Figure 12.** Cyclic voltammetry of **3** in $CH_2Cl_2$ with 0.05 M $n$Bu$_4$NPF$_6$ electrolyte; sweep rate of 0.5 V/s; reductive direction swept first.

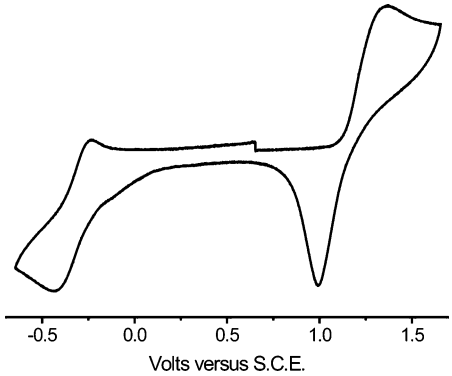


**Figure 13.** Cyclic voltammetry of **4** in $CH_2Cl_2$ with 0.05 M $n$Bu$_4$NPF$_6$ electrolyte; sweep rate of 0.5 V/s; oxidative direction swept first.

(31) (a) Chaudhuri, P.; Verani, C. N.; Bill, E.; Bothe, E.; Weyhermüller, T.; Wieghardt, K. *J. Am. Chem. Soc.* **2001**, *123*, 2213. (b) Cangiotti, M.; Formica, M.; Fusi, V.; Giorgi, L.; Micheloni, M.; Ottaviani, M. F.; Sampaolesi, S. *Eur. J. Inorg. Chem.* **2004**, 2853. (c) Kirk, M. L.; Shultz, D. A.; Depperman, E. C. *Polyhedron* **2005**, *24*, 2880.

**Table 2.** Summary of Redox Processes Observed by CV in $CH_2Cl_2$ with 0.05 M $nBu_4NPF_6$

| processes[a] | 1 | 2 | 3 | 4 | $Mn(hfac)_2(THF)_2$ | $Cu(hfac)_2(THF)_2$ | $Co(hfac)_2(THF)_2$ |
|---|---|---|---|---|---|---|---|
| first $E_{1/2}$(ox) | 0.84 | 1.16 | 0.07 | 1.18 | n/a | −0.06[b] | n/a |
| first $E_{ox}$ | na | 2.17 | 1.03 | na | 2.05 | 1.11 | 2.13 |
| second $E_{ox}$ | na | na | 1.40 | na | na | 1.45 | na |
| $E_{re-red}$ | na | na | 1.07 | na | na | na | na |
| first $E_{1/2}$(red) | −0.86 | −0.30 | −0.84 | −0.30 | na | na | na |
| first $E_{red}$ | na | −0.89 | na | na | −0.81 | −1.08 | −1.72 |

[a] Redox processes are labeled assuming an initial potential of 0 V and an oxidative sweep followed by a reductive sweep. Values in the table are quoted in V vs SCE. $E_{1/2}$(ox) and $E_{1/2}$(red) are the half cell potentials of reversible oxidative and reductive processes. $E_{ox}$ and $E_{red}$ are the potentials at maximum current for non-reversible processes. $E_{re-red}$ are the potentials at maximum current for processes occurring upon return oxidative scans that appear not to be part of a reversible process. [b] The oxidative process is at positive potential and the reductive process is at negative potential. We have chosen to list this as a reversible oxidative process to provide better tabular comparison with the copper complex **3**.

The first oxidation peak is the one-electron oxidation of the DTDA moiety, $[Mn^{II}DTDA^{\bullet}]^0/[Mn^{II}DTDA^{+}]^{+}$. If the applied potential is reversed at this point, then reduction regenerates the neutral complex. Compared with the free ligand **1** ($E_{1/2}$(ox) = 0.84 V in $CH_2Cl_2$),[9] oxidation of the coordinated ligand in **2** is at a higher potential. Furthermore, this process generates a redox wave with a greater difference between the oxidative and reductive potentials in the complex ($\Delta E_{ox-red}$(**2**) = 0.25 V) than in the free ligand ($\Delta E_{ox-red}$(**1**) = 0.18 V). Nevertheless, this demonstrates that the complex remains intact upon oxidation. When the oxidative potential is further increased, a second peak results from the oxidation of the manganese, $[Mn^{II}DTDA^{+}]^{+}/[Mn^{III}DTDA^{+}]^{2+}$. The potential of this peak is similar to the oxidative potential observed for the $Mn(hfac)_2(THF)_2$ species in $CH_2Cl_2$ (2.05 V). This second oxidation is followed by a relatively quick rearrangement of electron distribution, possibly generating a more stable $[Mn^{IV}DTDA^{\bullet}]^{2+}$ complex. On the return sweep, the neutral complex is regenerated by a two-electron reduction (e.g., $[Mn^{IV}DTDA^{\bullet}]^{2+}/[Mn^{II}DTDA^{\bullet}]^0$). Again the data suggest that the complex remains intact. Upon cycling of this redox process, no decomposition is observed.

As the neutral complex **2** is reduced, two reduction waves are observed at −0.37 and −0.89 V, respectively. On the return sweep, two smaller re-oxidation waves are observed. If the reduction sweep is reversed before observation of the second redox process, the first reduction wave becomes reversible ($E_{1/2}$(red) = −0.30 V). Based on reversibility, it is likely that this first redox process is ligand-centered; however, it should be noted that it occurs at a significantly more positive potential than either the fully reversible $E_{1/2}$(red) = −0.86 V process observed for **1** in $CH_2Cl_2$ or the irreversible $E_{red}$ = −0.81 V process observed for $Mn(hfac)_2(THF)_2$ in $CH_2Cl_2$. There is also a small temperature- and concentration-dependent irreversible peak observed at −0.10 V upon reduction when the oxidative potential is swept first. A similar peak is observed in the CV of the free ligand and may be attributed to intermolecular interaction, perhaps the onset of dimerization, in solution.

The CV of **3** is quite different in appearance from that of **2**. It is dominated by a broad reversible redox peak centered at $E_{1/2}$(ox) = 0.07 V. This is likely a metal-centered redox process, considering that the CV of $Cu(hfac)_2(THF)_2$ in $CH_2Cl_2$ reveals a quasi-reversible peak with $E_{ox}$ = 0.17 V and $E_{red}$ = −0.29 V. A second reversible peak is also observed in the reductive sweep at $E_{1/2}$(red) = −0.84 V. The difference in measured current (reduction as compared to reoxidation) in the voltage regime between these two reversible peaks suggests there may be another redox process in the reductive sweep. The oxidative part of the sweep reveals two peaks at $E_{ox}$ = 1.03 and 1.40 V, respectively. These are not reversible processes, but a small peak at $E_{red}$ = 1.07 V is observed upon re-reduction in the return sweep. Clearly the redox manifold of the copper complex **3** is much more complex than that of the manganese complex **2**. None of the redox processes can be unambiguously assigned as ligand-only processes, which may suggest a very different frontier molecular orbital manifold from that of **2**. This warrants further study, perhaps by combining solution EPR and CV measurements.

Cobalt complex **4** generates a simple CV with one reversible oxidation peak at $E_{1/2}$(ox) = 1.18 V and one reversible reduction peak at $E_{1/2}$(red) = −0.30 V. The oxidation peak is similar in appearance and position to the first oxidation peak of complex **2**. This implies that the process involved is the same as that in **2** and is most likely the oxidation and re-reduction of the coordinated ligand, $[Co^{II}DTDA^{\bullet}]^0/[Co^{II}DTDA^{+}]^{+}$. Increasing the oxidative sweep potential reveals no more peaks prior to the oxidation of the solvent. The reduction peak is similar in position to the quasi-reversible reduction peak observed in **2**; however, better reversibility of this peak is observed. This implies a process involving reduction and re-oxidation of the ligand such that the complex remains intact, $[Co^{II}DTDA^{\bullet}]^0/[Co^{II}DTDA^{-}]^{-}$. As with complex **2** and the free ligand, there is a small concentration- and temperature-dependent peak at −0.10 V that may be attributed to intermolecular interactions. There do not appear to be any metal-centered redox processes, which is in keeping with the CV of $Co(hfac)_2(THF)_2$ in $CH_2Cl_2$ wherein no redox processes are observed between −1.5 and 2.0 V (see Supporting Information).

## Discussion

The three different modes of solid-state packing observed for complexes **2**−**4** can be correlated to the differences in metal site geometries. The crystal structure of the Mn complex **2** reveals pseudo-trigonal ligand coordination symmetry about the manganese atom in one of the crystallographically distinct molecules and a highly distorted coordination symmetry, that qualifies neither as pseudo-trigonal nor as pseudo-octahedral, about the manganese atom in the other crystallographically distinct molecule. For a high spin

$d^5$ metal ion, there is no ligand field stabilization energy, so there is no particular favoring of pseudo-octahedral ligand distribution over any other geometry. Thus the hfac ligands do not sterically inhibit the dimerization of the molecules via *cis*-cofacial interaction of the DTDA ligands. By contrast, the dimerization mode observed in the crystalline state of the Cu complex **3** is a twisted-cofacial interaction. The pseudo-octahedral ligand coordination symmetry about the copper atom places the hfac ligands further above and below the plane of the DTDA ligand, a position that generates some steric hindrance to dimerization. The pseudo-Jahn Teller distortion typical of hexa-coordinate $d^9$ metal ions relieves enough of the steric bulk to allow dimerization in the twisted-cofacial mode. The lack of dimerization in the solid-state structure of the Co complex **4** is a result of the undistorted pseudo-octahedral ligand coordination symmetry about the cobalt ion, typical of high spin $d^7$ ions, which places the hfac ligands in a position that sterically blocks all modes of dimerization.

Another important point is that the long coordination axis about the copper ion in **3** is perpendicular to the plane of the DTDA ligand, elongating Cu−O bonds to the hfac ligands. This suggests that the DTDA nitrogen atom is a relatively good donor and that **1** is a "good" ligand. Sublimation of intact complexes **2** and **4** under static vacuum in high yield suggests the same. This is worth noting since many paramagnetic ligands, such as those derived from nitroxides, are comparatively poor ligands giving rise to metal complexes that are not particularly robust.

Information regarding the nature and magnitude of the exchange coupling between the ligand spin and the metal spin in **2** and **3** cannot be obtained from the solid-state DC-SQUID magnetometry measurements owing to crystal packing that generates a closed shell ligand dimer. We have used Evans' method magnetometry in order to obtain solution data for these complexes in an effort to glean some information regarding the intramolecular exchange coupling. We are aware that it is likely that a monomer/dimer equilibrium exists in solution and that this will complicate the interpretation of the solution magnetic data. To address this issue, we have used TD-DFT calculations in order to predict the differences in visible absorption spectra between the monomer and dimer of ligand **1**, according to the crystal structure geometries. Calculations predict an intense absorption at ca. 450 nm that arises from a dimer-HOMO to dimer-LUMO excitation and is thus absent in the monomer. We have measured the visible absorption spectra of **1**−**4** in solution as a function of temperature, tracking the intensity of a peak at ca. 450 nm. We are aware that there are several possible ligand dimerization modes, as we have observed in the crystalline state, and we suspect that there is, in fact, a much more complex dimerization equilibrium involving contributions from all possible dimer modes in solution. We are assuming that similar excitations in the visible region will accompany each of these modes and that measuring the broad absorption observed in this region for all four species is a reasonable way of quantifying the dimer concentration in solution. Furthermore, it should also be noted that, although the cobalt complex **4** is not dimerized in the crystalline state, an absorption in the visible region is detected at low temperatures in solution. This suggests that dimerization is possible in solution for this species.

From the solution absorption data, we have determined the monomer/dimer equilibria for all four species in toluene as a function of temperature. We find that, for **2** and **3**, there is a significant contribution from the dimer in solution, even at room temperature. For the free ligand **1**, the equilibrium lies more in favor of the monomer at room temperature, which is somewhat surprising based on steric arguments alone. Evidently, coordination of the metal ions influences other factors (e.g., electron distribution) contributing to dimer formation. Finally, the monomer/dimer equilibrium for **4** lies heavily in favor of the monomer at room temperature, as would be expected given the absence of dimer formation in the crystalline solid.

It is worth noting that the observation of dimerization for many varieties of thiazyl radicals in the solid state, and the possibility of monomer/dimer equilibria in solution, have been long-standing issues in the study of these heterocycles.[32] A good example for comparison with our results is the variable temperature EPR study of the $PhCN_2S_2$ radical in toluene from which thermodynamic parameters of dimerization have been evaluated as $\Delta H^\circ/R = -4200$ (in K) and $\Delta S^\circ/R = -14$.[33] These values are very similar to those we report herein for our species **1**−**4** and lend credibility to our results.

With the monomer/dimer equilibrium information afforded by our absorption spectroscopy studies, it is somewhat easier to interpret the solution magnetometry results. Complex **4** is not dimerized in the solid state, nor is there significant contribution from dimers in solution at temperatures above 250 K. It is not surprising, then, that the solution and solid state $\chi T$ values are the same, within error, in the 300 to 250 K regime. As the temperature is lowered further, the $\chi T$ values begin to decrease in solution, more dramatically and at higher temperature in $CD_2Cl_2$ than in toluene. This is likely associated with the onset of dimerization in solution, and ultimately precipitation in the case of $CD_2Cl_2$ as a solvent. From the solid-state magnetometry data, we have determined that the intramolecular exchange coupling is ferromagnetic (FM) for **4**, so dimerization should result in a decrease in $\chi T$ values, as observed.

For complex **2**, the solution $\chi T$ values in both $CD_2Cl_2$ and toluene are lower than the solid-state values at ambient temperature and increase upon cooling, reaching a maximum value roughly equivalent to the solid-state value. A simple orbital overlap model would predict antiferromagnetic (AFM) coupling between the ligand spin, localized in a $\pi^*$ molecular orbital, and the metal spin, with significant spin density assigned to d orbitals that are non-orthogonal to the ligand

(32) (a) Burford, N.; Passmore, J.; Schriver, M. J. *J. Chem. Soc. Chem. Commun.* **1986**, 140. (b) Brooks, W. V. F.; Burford, N.; Passmore, J.; Schriver, M. J.; Sutcliffe, L. H. *J. Chem. Soc. Chem. Commun.* **1987**, 69. (c) Awere, E. G.; Burford, N.; Mailer, C.; Passmore, J.; Schriver, M. J.; White, P. S.; Banister, A. J.; Oberhammer, H.; Sutcliffe, L. H. *J. Chem. Soc. Chem. Commun.* **1987**, 66.

(33) Fairhurst, S. A.; Johnson, K. M.; Sutcliffe, L. H.; Preston, K. F.; Banister, A. J.; Hauptman, Z. V.; Passmore, J. *J. Chem. Soc. Dalton Trans.* **1986**, 1465.

$\pi$ system. Without accounting for possible changes in $g$, one would then expect a higher $\chi T$ value for the dimerized complex in the solid state ($S = 5/2$ for one uncoupled $Mn^{2+}$ ion per molecule) than for the complex in solution which now has significant contributions from monomers ($S = 2$ ground state). As the temperature is lowered, the monomer/dimer equilibrium shifts dramatically in favor of the dimer such that, in toluene, the dimer contribution is roughly 4 orders of magnitude higher than the monomer contribution at 200 K. Thus, $\chi T$ values at low temperature in solution are roughly equivalent to those in the solid state. In the case of $CD_2Cl_2$, the $\chi T$ values drop again as the temperature is lowered due to the onset of precipitation of the solute.

For complex **3** at ambient temperature, the solution $\chi T$ values are higher than those of the solid state, and markedly so for toluene as a solvent. A simple orbital overlap model predicts intramolecular FM coupling since the metal spin is localized in a d orbital that is orthogonal to the ligand $\pi$ system. Assuming the absence of a dramatic decrease in $g$, a larger $\chi T$ value is expected for a solution of **3** with significant contribution from the monomer ($S = 1$ ground state) than for the solid state in which the complex can be treated an uncoupled $Cu^{2+}$ ion ($S = 1/2$), owing to the absence of spin on the ligand due to dimerization. As the temperature is lowered, the $\chi T$ values in solution drop, likely with the shift in monomer/dimer equilibrium in favor of the dimer. In the case of $CD_2Cl_2$, the $\chi T$ value drops below the solid-state value, consistent with the observation of precipitation of the solute at very low temperature. We speculate that the solvent dependence of the solution $\chi T$ values may be due to solvent dependence of the monomer/dimer equilibria. Unfortunately, we are unable to confirm this hypothesis, beyond pointing to observed differences in solubility at low temperatures, because partial evaporation of the extremely volatile $CD_2Cl_2$ from cells employed for variable temperature visible absorption spectroscopy made it impossible to accurately define the concentration of the solution.

We have refrained from attempting to quantify the intramolecular exchange coupling in **2** and **3** based on the information presented here for a number of reasons. The solution magnetometry is limited to a relatively high-temperature regime owing to restrictions imposed by solvent freezing points. This regime tends to be dominated by contributions from $g$, rather than from exchange coupling, in part because thermal excitations can lead to occupation of excited spin states so the ground state spin configuration is typically not the exclusive contributor. Although, in principle, one could subtract the dimer contribution to the solution $\chi T$ values based on the known equilibria and the measured solid-state values, one would have to assume, perhaps erroneously, that the $g$ value associated with the dimer in the solid state is roughly the same as that of the monomer in solution in order to make any further estimates. Finally, there is inherent error in each of these measurements and the accumulation of this error in the final calculation, taking solid state, solution state, and equilibrium values into consideration, would be great, generating values of tenuous significance at best. Thus, we have chosen to discuss observed trends rather than calculating actual values for the exchange coupling. Nevertheless, it appears that the exchange coupling between the ligand spin and the metal spin is as might be predicted; AFM in for **2** and FM for **3**. Furthermore, given that the monomer/dimer equilibrium constant in solution at ambient temperature is close to unity, so the monomer contribution to the solution $\chi T$ values is "diluted", and given that thermal occupation of excited spin states further "dilutes" the contribution of the monomer ground state spin configuration to the $\chi T$ values, the fact that we observe the above trends suggests that the magnitude of the exchange coupling is relatively large. This is as expected given that the metal ions are coordinated to a DTDA nitrogen atom with significant spin density.

We have also investigated the solution and solid-state X-band EPR spectra of **2** and **3** and the CV profiles of solutions of **2**−**4** in an effort to further characterize these species. The CV measurements of **2** suggest that there may be oxidation states of the manganese complex that are accessible via chemical redox processes. This is worth investigating in future studies. While complex **4** appears to be relatively uninteresting in terms of its electrochemistry, CV profiles of **3** reveal a complex redox manifold. This, too, may be worth further investigation, either computationally or chemically. Finally, the EPR spectra of **2** and **3** have not contributed any significant understanding to the exchange coupling in these species.

## Conclusion

The 4-(2′-pyridyl)-1,2,3,5-dithiadiazolyl radical **1** is a versatile bidentate N-coordinating ligand capable of forming robust complexes with dications of several first row transition metals ($Mn^{II}$, $Co^{II}$, and $Cu^{II}$). Subtle differences in coordination geometries can influence the solid-state packing of the complexes, such that the Mn complex **2** and the Cu complex **3** form dimers through close S···S contacts in the solid state, whereas Co complex **4** is undimerized in the solid state. We have determined values for the solution monomer/dimer equilibria of these complexes and used this information to interpret the solution magnetic susceptibilities of these species. It appears that, in keeping with the previously reported solid-state magnetometry observations of complex **4**, the exchange coupling between the spin on the DTDA ligand and that on the coordinated metal ion is relatively large and predictable in nature using a simple orbital overlap model.

**Acknowledgment.** We thank D. A. Shultz at North Carolina State University for access to his DC-SQUID magnetometer. K.E.P. thanks the Natural Sciences and Engineering Research Council of Canada, the Canada Foundation for Innovation, the Ontario Innovation Trust, and the University of Guelph for funding. N.G.H.R. thanks the Ontario Graduate Scholarship for funding.

**Supporting Information Available:** Crystallographic information files (CIF) for **2** and **3**. Variable temperature visible absorption spectra for **1**, **2**, and **4** in toluene. Solid-state X-band EPR spectrum and solution spectra in $CH_2Cl_2$ and $CHCl_3$ of **3**. CV plots of $M^{II}(hfac)_2 \cdot 2THF$ (M = Mn, Cu, Co) in $CH_2Cl_2$. This material is available free of charge via the Internet at http://pubs.acs.org.

IC0619456